Near Net Shape Casting: Is It Possible to Cast Too Thin?

CARL SLATER and CLAIRE DAVIS

With increased efforts across the steel industry to produce steel in more economical ways, interest in near net shape casting has increased. Although much has been reported on the production of exotic alloys *via* these methods, to make the investment in new casting equipment, capability to produce current high value steels by these methods would derisk the capital expenditure. This study assesses the production of a dual phase steel (DP800) by belt casting and compared to that of conventional continuous casting. Although a drop in yield and tensile strength was seen in the belt cast-produced material, the increased elongation allowed for a comparable/improved UTS × elongation factor. A combination of *in situ* dendrite measurements, thermal modeling, and lab-scale belt casting has allowed insight into the relationship between cast thickness and final band spacing. The inherent lack of deformation of near net shape casting results in coarser band spacing and is not accounted for by the refinement of the secondary arm spacing caused by the faster solidification rates. This limits the strength achievable for a given martensite volume fraction. This has been predicted across the full range of casting thicknesses (1 to 230 mm) and good agreement has been shown with experimental results.

https://doi.org/10.1007/s11663-020-01964-z

I. INTRODUCTION

NEAR net shape casting technologies such as twin roll and belt casting have both made huge strides in commercialization in the past decade. Ventures such as the joint SMS Seimag/Salzgitter Flachstahl,[1] the new Castrip facilities in China (completed 2019) and the USA (building commenced 2016),[2–4] have all seen step changes towards commercial production through these rapid, more cost-effective methods. A major attraction for development and increasing implementation of these processes lies in their energy efficiency, with technologies such as horizontal belt casting showing potential energy savings > 3 GJ/ton of steel produced.[5,6] Another advantage is the system size and casting speed with near net shape casters being 8 to 10 times smaller and capable of casting speeds up to × 150 faster compared to thick slab continuous casting routes.[1,6]

One of the additional potential drivers of these techniques is the ability to produce new or exotic alloys that previously were ''uncastable'' by conventional continuous casting. These alloys included high manganese TWIP/TRIP grades,[1,7–10] high silicon electrical steels,[11–13] high carbon energy efficient sheets,[14] as well as ultra-thin HSLA grades.[15] However, with the exception to the TWIP/TRIP, these have been lab/pilot scale in the majority. While each of these show promising developments, none are without their problems (such as surface quality, centreline position *etc.*[16]), but also the expected production volumes (with the exception to maybe the electrical steel) are low in comparison to the more commodity grades. Current usage of some of the commercial net shape production has been for the more commodity grades, which although proves that the technology will not compete with the larger scale mass production of continuous casters. The question remains that for these new casting methods to become more commercially viable and for greater adoption, do they need to be able to produce a wider range of higher value conventional grades (HSLA, AHSS *etc.*) to at least the same quality of conventional continuous casting? As the majority of the work on these processes have been lab based, there is little in the way of benchmarking against conventional continuous casting; however, some literature suggest that the net shape route produces a coarser microstructure as seen by Kwon *et al.*[17] in ferritic high-aluminum alloys, where the conventional ingot route showed nearly a 10 pct higher UTS compared to the a twin roll cast counterpart.

CARL SLATER and CLAIRE DAVIS are with the WMG, University of Warwick, Warwick CV4 7AL, UK. Contact e-mail: c.d.slater@warwick.ac.uk
Manuscript submitted May 24, 2020.
Article published online September 28, 2020.

The batch type production of the near net shape processes lends itself well to switching between alloys, and therefore, understanding the metallurgical impact of producing the commodity grades through this route is needed.

II. MATERIALS AND METHODOLOGY

A benchmark AHSS material was selected to compare to belt cast production of the same composition; this is a commercial DP800 produced as thick (230 mm) slab using continuous casting with a composition of 0.13C-1.85Mn-0.55Cr-0.25Si and a product thickness of 1 mm.

Two casts were made to replicate strip produced *via* single horizontal belt casting. This was achieved using a 10 kg vacuum induction melting furnace (VIM) pouring into a horizontal mold with an argon gantry system which gives the asymmetric cooling seen in full-scale production (Figure 1). 4 kg of steel with nominally the same composition (residual elements in lab casts < 50 ppm) as the commercial benchmark grade was melted inside the crucible; once the molten steel reached the desired pouring temperature, the steel was poured into the mold and simultaneously the top quench argon was switched on at a flow rate of 0.5 L/min. Thermal imaging was used to measure the cooling rate of the surface of the cast material. This process produces a cast ingot of 250 × 80 mm with a strip thickness of 10 mm.

During casting *via* single horizontal belt casting, the range of pour temperatures achievable is greater than that of conventional continuous casting. This is due to the pouring temperature during continuous casting needing to balance between being low enough to achieve a sufficient solidified shell thickness to support the liquid steel on exiting the mold, but high enough to avoid clogging the submerged entry nozzle into the mold. As belt casting is a horizontal process with flow onto the belt, the constraint on containing the liquid is much less, and therefore, higher super heats can be used, the lower temperature limit to avoid clogging is similar. Therefore, a 5 °C and 100 °C superheat was used to explore the full range of initial cast microstructures available by belt casting and the effect this has on the subsequent microstructure development during rolling and heat treatment.

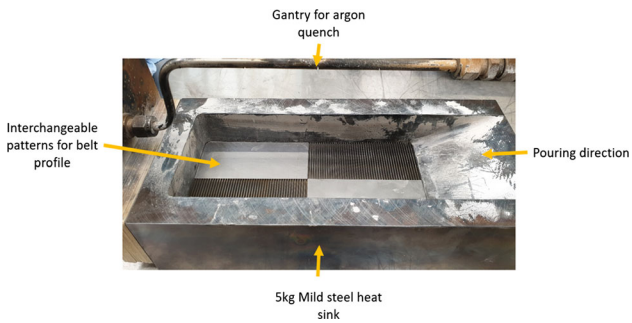

Fig. 1—Image of the mold used to replicate single horizontal belt casting inside the vacuum induction melting furnace.

After casting the material underwent a standard reheat cycle of 1250 °C for 2 hours and then was hot rolled to 3 mm (typical for a hot band product) through 4 passes at 1050 °C, with the hot rolled strip subsequently cooled slowly in order to obtain the typical ferrite/pearlite structure prior to cold rolling. The hot band strip was then cold rolled to a final product thickness of 1 mm.

The final cold rolled samples were then heat treated along with the commercial product. The commercial product was heat treated as the exact commercial intercritical annealing cycle is unknown, and therefore, in order for the two sets to be comparable then identical heat treatments have been given to all samples prior to tensile testing. For intercritical annealing, a temperature of 820 °C for 2 minutes was used and quenched to form the characteristic martensitic/ferritic structure. This time and temperature profile is typical for similar compositions where a 40 pct martensite volume fraction is required.[18] Although an average temperature is normally applied to temper the martensite, here, the quenched condition will allow a greater insight into the microstructural differences between the casting routes.

After heat treatment, longitudinal and transverse tensile specimens were machined from the strips using electric discharge machining (EDM).

Confocal scanning laser microscopy (CSLM) was carried out on a Yonekura VL2000DX-SVF17SP CSLM using a 2 × 2 × 2 mm section to consider the effect of cooling rate (from belt casting to thick slab continuous casting rates) on microstructure development. The chamber was vacuumed and refilled with N6 argon three times before each test. Samples were then heated at 10 °C/s to 1550 °C and held for 2 minutes. The sample was then cooled at a series of cooling rates between 0.1 and 20 °C/s before remelting by heating back up to 1550 °C. Video recording was carried out at 30 Hz and secondary dendrite arm spacing was measured from a minimum of 50 length measurements for each cooling rate.

SEM microscopy was carried out on the 10 mm lengths of each sample. Samples were sectioned and polished down to a 0.25 μm finish. SEM was then carried out on a JOEL 7800F.

Tensile testing was performed on a 30 kN Instron machine using standard ASTM370 subsize sample geometry. The samples had full thickness with a gauge width of 6 mm. A 25 mm clip extensometer was used, and tests were deformed out at 2 mm/min until failure according to ISO 6892-1:2016.

III. RESULTS AND DISCUSSION

A. *Confocal Microscopy*

There are two major differences between conventional thick/thin slab continuous casting and near net shape casting that affect the microstructural development: the level of deformation needed between cast slab/strip and final product and the solidifying cooling rate during casting. To understand the impact of the latter, an understanding of the solidification and segregation behavior is needed.

As most steels undergo at least one solid-state transformation after solidification before reaching room temperature, obtaining secondary dendrite arm spacing (SDAS) generally relies on using fast cooling rates to room temperature and then etching to reveal the SDAS, with the etchant selected depending on the composition of the steel. In this study, CSLM has been used to directly observe the solidifying steel, which allows a much more rapid assessment of SDAS and fine control of the cooling rate through solidification. A previous study has shown that the surface measurements of SDAS in the CSLM are the same as observed in the bulk material.[19]

Figure 2 shows the secondary dendrite arm spacing (SDAS) as a function of the cooling rate and a typical image of the steel surface in the CSLM where the solidifying steel secondary dendrite arm tips can be seen; as the dendrite grow approximately parallel to the steel surface, the spacing between the observed tips gives the SDAS.[19] The SDAS with cooling rate data has been compared to the literature[20] for a similar steel (0.17C-1.5Mn-0.4Si) and good agreement between the two can be seen in Figure 2. The obtained relationship between SDAS and cooling rate (CR) from this work is given as follows:

$$\text{SDAS} = 70\,\text{CR}^{-0.5} \quad [1]$$

Although many broader equations exist for predicting SDAS, such as those that include compositional influences (particularly carbon),[20,21] here, a simplified approximation has been used that will apply for this specific alloy across the full range of cooling rates tested.

B. *Prediction of Microstructural Variable Due to Cast Thickness*

As the dendritic structure shows such sensitivity to cooling rate, understanding the cooling rate as a function of cast thickness is needed to consider differences between belt cast and thick/thin slab cast material. Particularly as it is known that the SDAS controls the segregation distribution in steel.[22,23] A COMSOL Multiphysics model was created to predict the cooling rate of casts produced with varying thickness from 240 mm (typical conventional thick slab continuous casting) down to 1 mm (twin roll casting). For the purpose of this study, then a constant boundary heat flux of 2.5 MW/m^2 was used. Although it is appreciated that for full through thickness analysis and in-depth studies of the initial stages of solidification, a more complicated heat flux profile is needed to represent aspects such as the columnar to equiaxed transition, grain size, and macrosegregation. However, many studies have shown that a value of 2 to 3 MW/m^2 is a good approximation for steady-state heat flux and thus appropriate for use when comparing 1/4 thickness cooling rate conditions. It should also be noted that the same heat flux values were experimentally found for twin roll casting,[24] belt casting,[16,25] and continuous casting.[26] Figure 3 shows a schematic of the COMSOL model where the red surfaces show the location the heat flux applied.

Figure 4 shows the resultant cooling rate as a function of cast thickness from the COMSOL model. Typical values for different strip casting methods have also been highlighted in Figure 4. It can be seen that from 240 down to 50 mm, very little difference in cooling rate at the quarter thickness position can be seen. The rate increases rapidly at thinner product approaching twin roll casting when the surface area to volume ratio increases and the thermal mass of the steel reduces.

Using Eq. [1], the cooling rates determined in Figure 4 can be converted to a SDAS with cast thickness, shown in Figure 5, giving a curvilinear trend with a greater sensitivity at the thinner strip end of the curve. Figure 5 also shows the literature values for as-cast SDAS for different continuous casting techniques. Here, only alloys with carbon concentrations within 0.04 wt pct of the target content have been selected. Although a reasonable amount of scatter can be seen (due to variations such as casting speed, mold fluxes *etc.*), the trend presented from the model agrees well with published data.

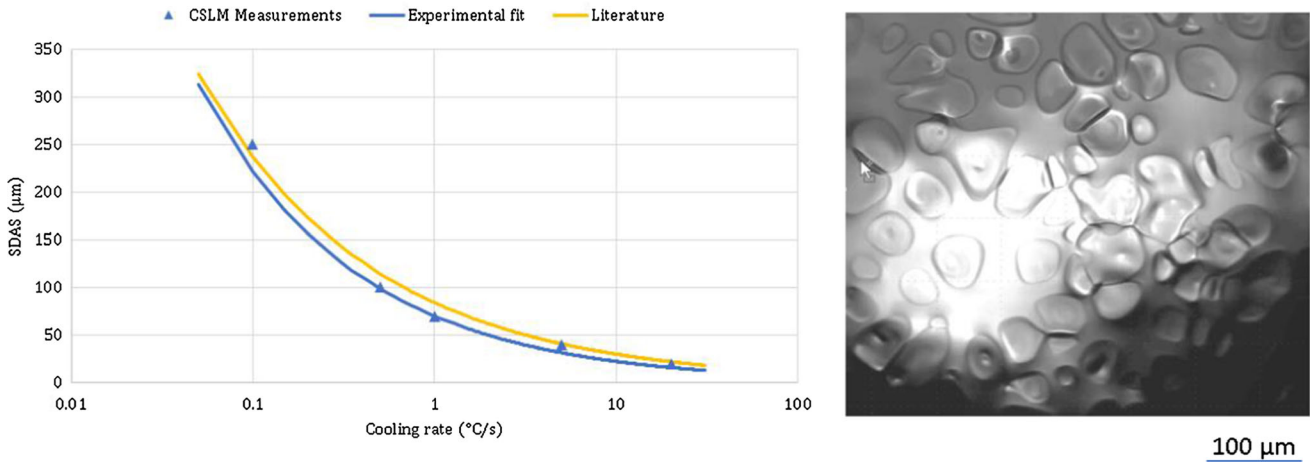

Fig. 2—Measured and literature-predicted SDAS as a function of cooling rate for DP800 determined using CSLM and an image of the solidifying steel surface showing the solid SDAS dendrite tips.

The final strip thickness is dictated by the product and, therefore, the customer requirements. This means that material that is cast thinner will require less rolling deformation to obtain the final thickness. Dual phase steels attribute much of their strength from the presence of a second phase (predominantly martensite) which typically present in bands in the product. These bands are originally linked to the segregation in the cast material (*e.g.*, Mn) and hence the SDAS and the band spacing are also affected by the amount of reduction (hot and cold rolling) to final thickness. Therefore, the final band spacing of the second phase can be approximately calculated as the SDAS divided by the amount of reduction to product thickness (in the case study considered in this work, to produce a 1-mm-thick final strip), and is shown in Figure 6. It can be seen clearly that the reduction in SDAS that is achieved at higher cooling rates cannot account for the vastly reduced amount of deformation that is needed to produce the final strip. Therefore, the thinner casts are expected to have an inherently larger band spacing than thick cast material.

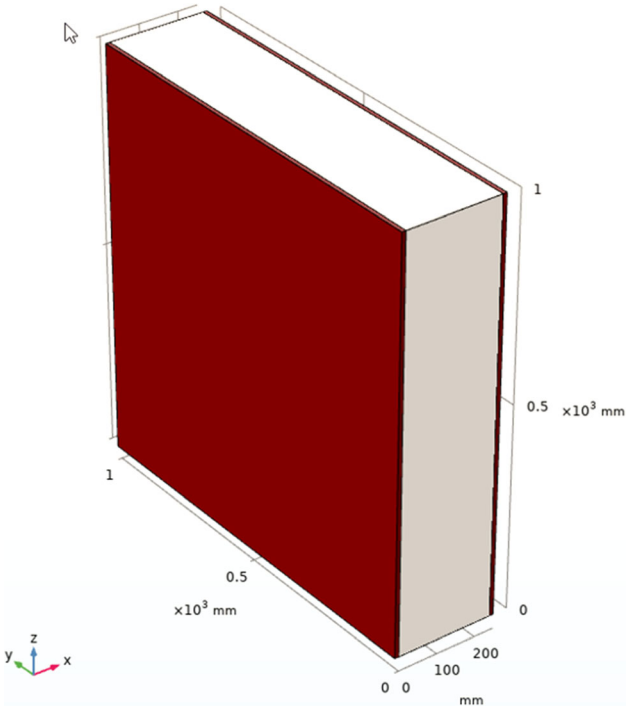

Fig. 3—Image taken from the COMSOL Multiphysics model used in this study. The red indicates the surfaces on which a constant heat flux of 2.5 MW/m^2 was applied.

Due to the intercritical annealing process, the cold deformed ferrite grains first go through a recrystallization phase before growing. The rate at which they grow is dictated by the time at temperature and the radius of the grain. This can be predicted through the following equation:

$$D_f^2 - D_0^2 = k_0 t^{0.48} \exp\left(\frac{Q}{RT}\right) \quad [2]$$

where D_f and D_0 are the final and initial grain size. k_0 is the preexponential factor and Q is the activation energy. A range of values exist for dual phase steels for Q and K_0; however, research by Zhu and Militzer[30] found the post-recrystallization growth constants Q and k_0 to be 325 kJ/mol and 1.2e5 m^4/J s, respectively. This suggests that any grains < 5 μm after recrystallization would grow to > 60 μm if unimpeded for a heat treatment of 820 °C for 120 seconds. This grain growth exceeds that of the band spacing; therefore, either the grains grow until impeded by a

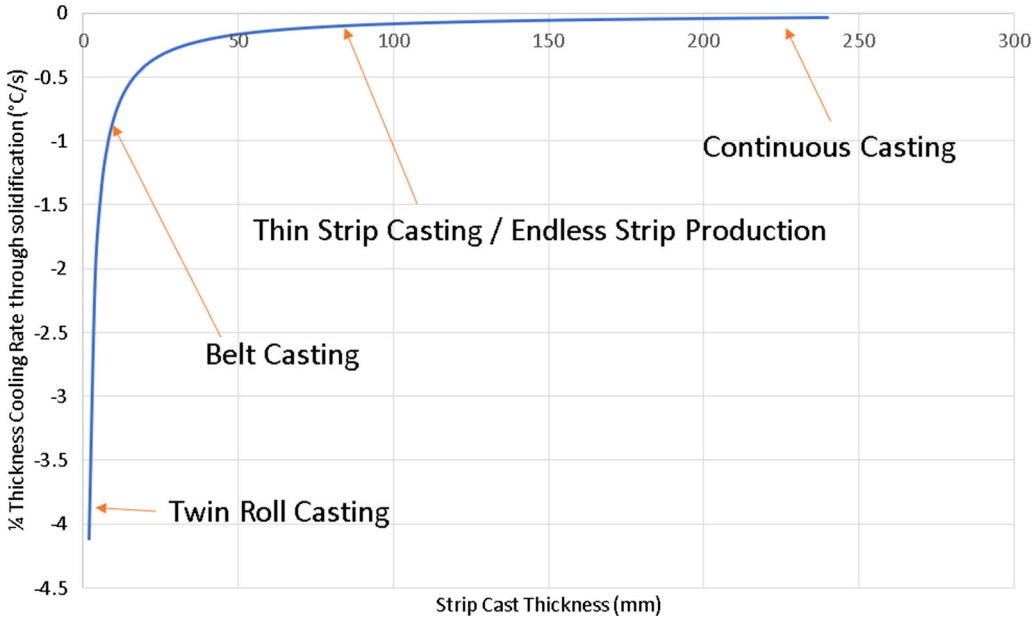

Fig. 4—Influence of cast thickness on the cooling rate at the quarter thickness position for different cast thicknesses. Typical values for different casting methods have been highlighted.

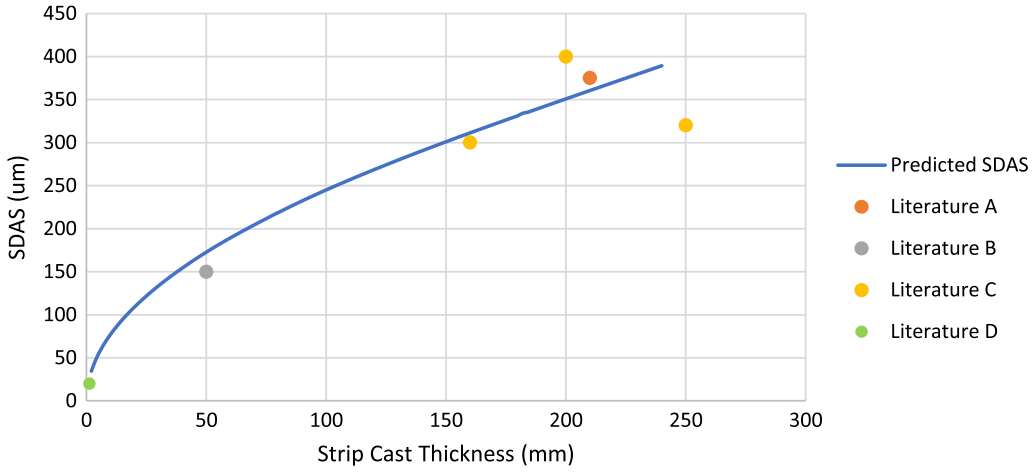

Fig. 5—Predicted SDAS of DP800 produced by casting to varying thicknesses compared with the literature values from A,[22] B,[27] C,[28] and D.[29]

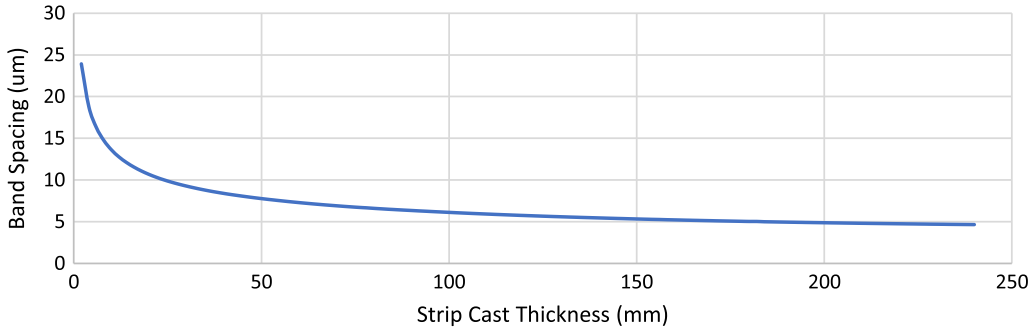

Fig. 6—Predicted band spacing of DP800 produced by casting to varying thicknesses.

growing austenite grain once transformation has started, or the ferrite grains grow to their potential and are consumed in the Mn-rich regions once the austenite starts to form. Either way the resultant ferrite grains are constrained to the band width in the normal direction. This suggests that casts that have had a greater level of deformation and, therefore, a finer band spacing will have an equally fine ferrite grain size.

C. *Microstructural Analysis*

Figure 7 shows the ferrite/pearlite microstructure of both the 5 and 100 °C superheat casts produced *via* laboratory scale belt casting after hot rolling to 3 mm. It has been seen in previous studies[31] that superheat has a significant impact on the grain size and morphology of a belt cast product. For large superheats coarse columnar microstructure is likely to dominate due to the strong thermal gradient through the billet. However, when superheats are much lower, this encourages an equiaxed structure. Although the SDAS is most heavily dictated by the cooling rate, the distribution and orientation of the dendrites in the initial cast is less uniform for lower superheats, which can be seen to transfer to the hot band products seen in Figure 7. The 100 °C superheat shows a strong alignment with the rolling direction, whereas the 5 °C, although starting to show signs of orientation in the rolling direction, remains less uniform.

Figure 8 shows the cold rolled samples from the casts with 5 and 100 °C superheats, respectively. Here, the initial variation in pearlite seen in Figure 7 has been significantly reduced. The further 3x reduction that has occurred during cold rolling is dominating the spatial distribution of pearlite. Both samples show almost continuous regions of pearlite across the image with some regions of coarser pearlite around 15 μm. After intercritical annealing (Figure 9), it can be seen that there is very little discernible differences between the casts. Table I shows the grain size and band spacing for the annealed samples and very little difference can be seen between the two belt casts, with the 100 °C superheat showing a marginally larger band spacing. The commercially produced sample, however, shows a significantly smaller grain size and band spacing; this is consistent with Figure 6 which suggested that even though the thinner grades will solidify much quicker, the level of reduction the thicker cast have will be the more dominant affect.

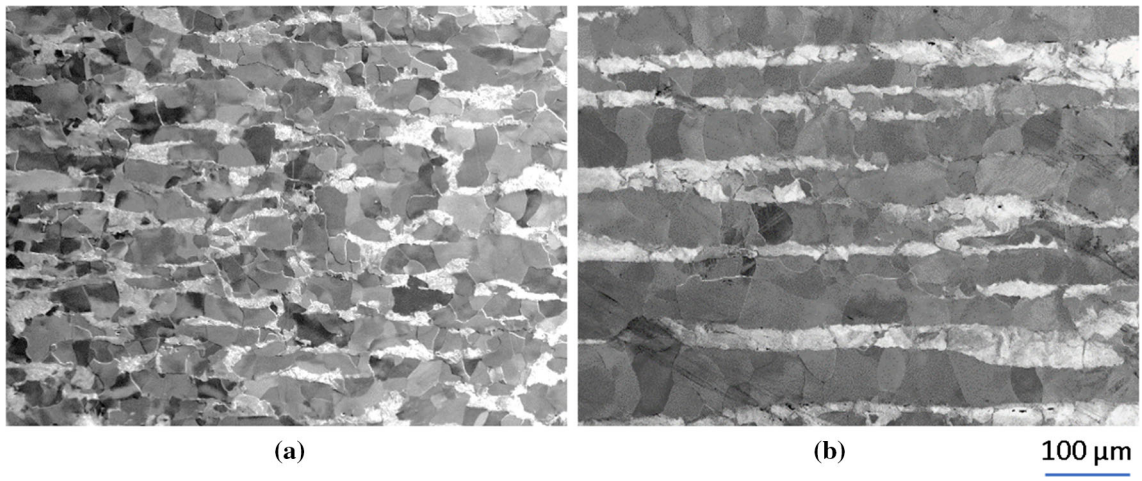

Fig. 7—SEM micrographs of the belt cast sample with (*a*) 5 and (*b*) 100 °C superheat after hot rolling.

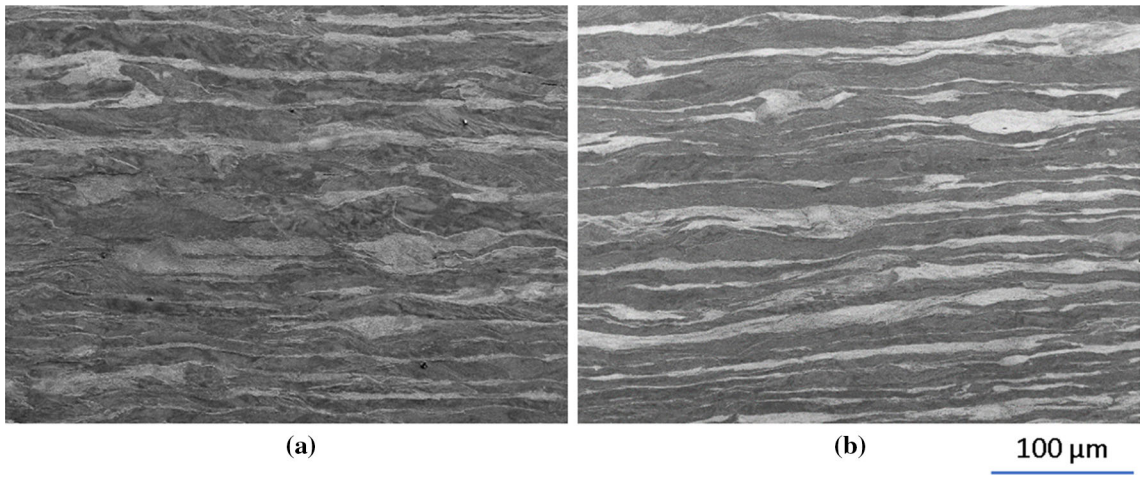

Fig. 8—SEM micrographs of the belt cast sample with (*a*) 5 and (*b*) 100 °C superheat after cold rolling.

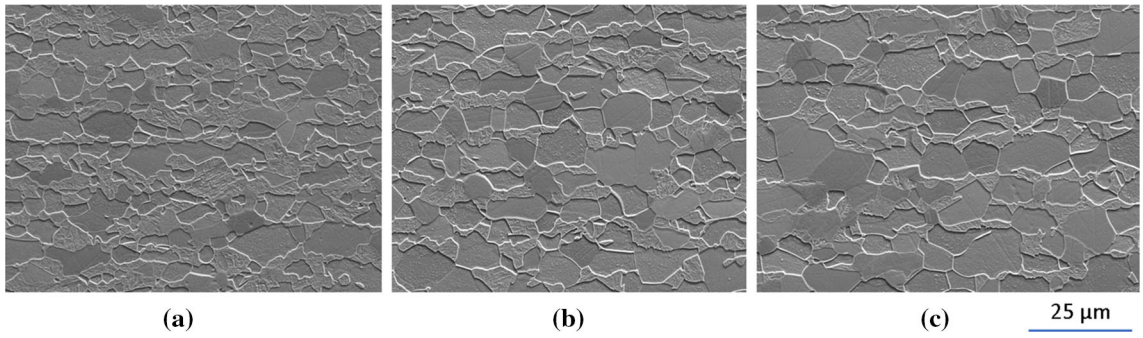

Fig. 9—SEM micrographs of (*a*) commercial benchmark DP800 grade, as well as the lab-produced belt cast samples at (*b*) 5 °C superheat and (*c*) 100 °C superheat.

D. *Tensile Testing*

The tensile curves from both the belt cast and the commercially cast steels after intercritical annealing can be seen in Figure 11 and summarized in Table II. Due to the nature of small VIM casting, these casts are typically cleaner than that of commercial. For this reason, yield, UTS, and uniform elongation were selected for comparison as total elongation and fatigue are more sensitive to these features. No significant difference can be seen between the belt cast samples using different superheat temperatures. This agrees well with the similarity in microstructures from the cold rolled stage

as well as after intercritical annealing. This suggests that although the mechanical properties of the final product produced *via* belt casting is not sensitive to superheat/cast morphology, aspects like the superheat can be chosen based on the optimization of other aspects such as surface quality, productivity *etc*.

Although no significant differences can be seen between the belt cast samples, a significant difference can be seen in the commercial product and the belt cast products in yield strength, UTS, and uniform elongation. This has also been seen in work by Xiong *et al*.[29,32] where a yield and UTS value showed to be as low as 350 and 560 MPa, respectively, when strip casting a dual phase steel (similar martensite fraction and composition as this study) to 1.2 mm; however, an increase in total elongation of around 10 pct was seen.

The increase in both UTS and yield for the commercial cast can be understood through the change reduction in grain size. Many studies have looked at the Hall–Petch relationship in dual phase steels;[33–35] however, the values of σ_o and k show a wide range due to the complex nature of dual phase steels. The yield stress and work hardening rate of dual phase steels are both dictated by the strain in the ferrite matrix caused by the martensitic transformation. This can vary because of many factors such as carbon concentration, volume fraction of martensite, and the distribution of that martensite. This makes predicting absolute values of dual phase steels difficult. Therefore, for the purpose of this study, the relative change in both yield and UTS with grain size has been assessed, which is much less sensitive to the literature variation in the Hall–Petch constants. The equations used can be seen below and fit within the range of that seen in the literature,[33–35] where D is the grain size taken from Table I.

$$\sigma_y = 400 + \left(1100 d^{-\frac{1}{2}}\right) \quad [3]$$

$$UTS = 700 + \left(1000 d^{-\frac{1}{2}}\right) \quad [4]$$

This gives a drop in yield and UTS of 225 and 210 MPa (± 30 MPa) when comparing the commercial product to the belt cast products. The measured difference between these cast was 240-260 MPa for yield strength and 250 to 300 MPa for UTS. This means that a significant portion of the difference between the two production routes, in terms of mechanical properties, is dictated by the grain size. Elongation, however, can be seen to have a significant improvement in the belt cast material for a given tensile direction. The consistent 30 to 50 pct increase in uniform elongation from the commercial product to the belt cast product is likely to be attributed to band spacing also. As martensitic bands are spaced further apart, the shear caused in the ferrite matrix due to these bands moving apart reduces for a given displacement. This allows for much greater elongation before failure, for a given longitudinal direction.

Dual phase steels show a linear relationship between UTS and Elongation throughout the range DP600 to DP960.[32] This can also be seen in these materials where the belt cast samples have either equal or improved UTS × uniform elongation (Table II). This suggests that although as a direct comparison (*i.e*., comparing alloys of similar martensite volume fraction), belt cast sample appear to underperform. However, if they are compared to that of a dual phase steel of equal tensile strength, the results suggest that they will be comparable, if not show a slight improvement in elongation. Although

Table I. Summary of the Ferrite Grain Size in All the Intercritically Annealed Samples Used in This Study

	Measured Grain Size (μm)*	Measured Band Spacing (μm)*
Belt Cast with 5 °C Superheat	9	10
Belt Cast with 100 °C Superheat	10	12
Commercial Grade	4	5

*± 0.5 μm.

Table II. Summary of the 0.2 Pct Proof Strength and UTS for the Three Strip Products in Both the Ferrite/Pearlite and Ferrite/Martensite Conditions

Test Sample	0.2 Pct Proof Strength (MPa)	UTS (MPa)	Uniform Elongation (Pct)	UTS × Uniform Elongation (MPa Pct)
Commercial-Long-FM	783	1169	2.6	3039
Commercial-Trans-FM	780	1165	3.4	3961
100C Superheat-Long-FM	540	912	3.4	3100
100C Superheat-Trans-FM	520	870	4.8	4176
5C Superheat-Long-FM	539	892	3.5	3122
5C Superheat-Trans-FM	538	914	4.2	3838

conventionally 20, 40, and 60 pct martensite fractions are used to created DP600, DP800, and DP1000, respectively, belt cast-produced materials achieve the same tensile strength/elongation ratio albeit with a different martensite volume fraction. This may limit the production of ultra-high strength DP steels, but suggest that current conventional dual phase steels can be produced through this cost-effective method.

Another feature that can be seen in Figure 10 is the difference between the longitudinal and transverse properties of all the products. The samples tested in this study has been in the as-quenched condition; this results in a high strain differential between the martensite and ferrite (commercially this would have been overaged to temper the martensite or even promote some bainite formation). Due to this, the strain is heavily dictated by the brittle martensite. Longitudinal samples that show almost continuous martensite colonies will be limited to the elongation of the martensite before decohesion/voiding occurs at the phase boundary. Conversely, the transverse samples will be dominated by the ferrite matrix, and thus, a much greater elongation is seen. This principle is common in unidirectional polymeric composites among others.[36]

From Figure 10 it is apparent that both the commercial and belt cast materials show no sign of discontinuous yielding. One of the main advantages of dual phase steels is its ability to prevent this region from occurring, which is detrimental to the forming and surface finish of sheet formed products. During cooling, after intercritical annealing, then the martensitic transformation causes transformational stresses in the ferrite at the interface with the martensite. This initially high locally level of dislocations is usually sufficient to suppress the region of discontinuous yielding and move straight into the work hardening stage of deformation.[37] The level at which the martensite can strain the ferrite matrix depends on the size, shape, volume fraction and carbon level of the martensite that is produced.[38] It has been shown that as the 2nd phase regions are spaced further apart or volume fraction reduces, the region of discontinuous yielding is broadened.[39] As the tensile curves in Figure 10 all show no discontinuous yield region, even for the belt cast samples, then it suggests that for the volume fraction, band spacing combination in these DP800, the transformation stress is sufficient to suppress the discontinuous yielding phenomena. This is consistent with Calcagnotto et al.[40] where even a coarse grained (12 μm) dual phase steel with 30 pct martensite did not see discontinuous yielding.

By bringing in the predictions from Figure 6, Eqs. [3] and [4], and the tensile results seen in Table II, the relative change in yield and UTS can be seen in Figure 11. The experimental belt cast steels produced in this study have been plotted alongside the commercial product. From this it is clear to see that the impact of accelerated cooling to thinner strip products has a noticeable detrimental effect on the yield and UTS of the material. This is true for both the experimental and predicted values, which are in good agreement. This suggests that although clear benefits are known with regards to the energy efficiencies of near net shape casting technologies, for grades that derive much of their mechanical properties from the deformation process, there is a cost in strength performance. This agrees well with literature where around a 30 pct reduction in UTS was seen in a dual phase steel cast to 1.2 mm.[32]

According to the cooling rates shown in Figure 4, and the reduction needed to convert a 10 mm cast section to a 1-mm-thick product, a cast SDAS of around 50 μm would be needed (nearly half the current SDAS) to achieve similar mechanical properties to that of a conventional continuous caster. Should accelerating the cooling rate be impractical, one of the following can be used to obtain the required properties:

- microalloying additions to refine the austenite grain size during hot rolling, given a finer cold rolled ferrite grain size while pinning the ferrite grains during intercritical annealing.
- Increase martensite fraction. As the net shape samples show increased elongation, increasing the martensite will readdress the yield/elongation balance required. This has been seen in Ref. 32 where a martensitic volume fraction/composition of a DP800 actually

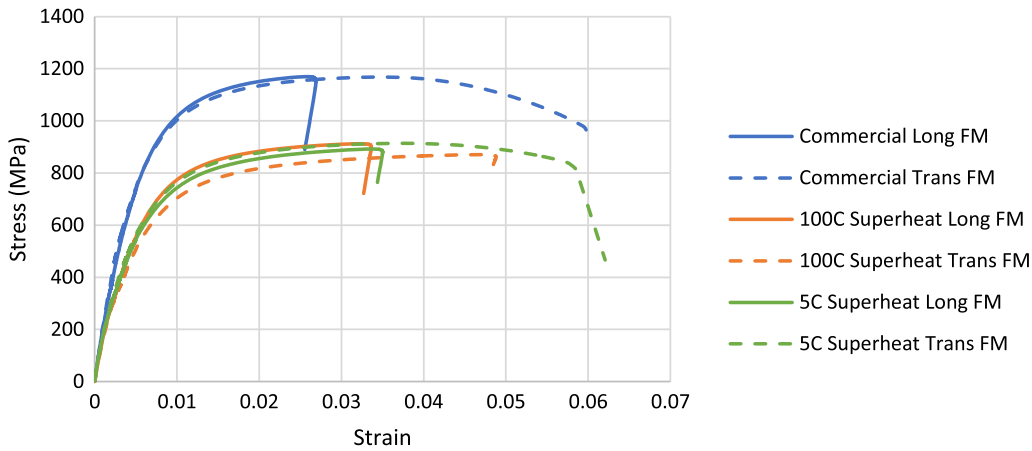

Fig. 10—Tensile stress/strain curves for the two belt cast strip and the commercial strip in the ferrite/martensite condition.

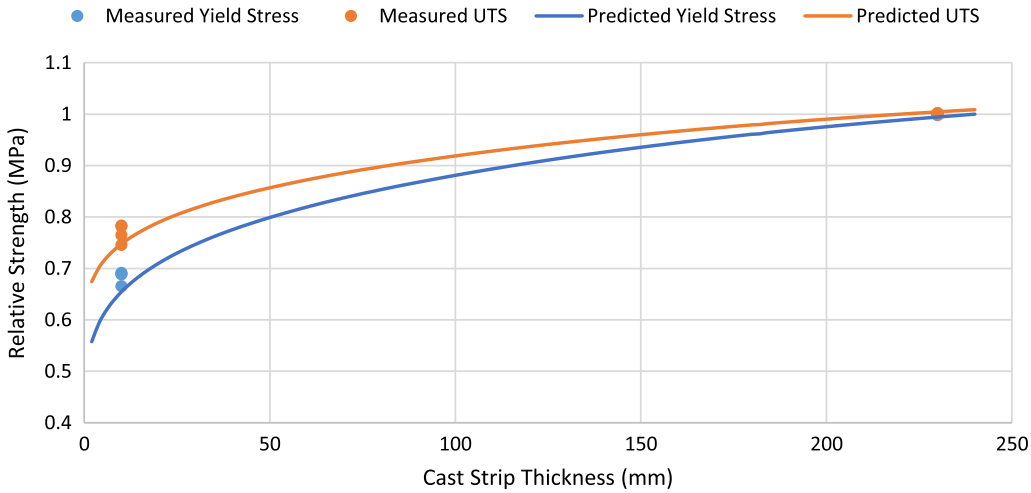

Fig. 11—Predicted and experimental measurements for yield stress and UTS for commercial and belt cast-produced products.

gives the same strength as a DP600, but with a slightly improved elongation (2–3 pct).

Although transitioning directly from continuous casting to near net shape casting initially appears to compromise performance. However, UTS × elongation of the belt cast samples show comparable performance and should the convention of volume fraction of martensite and strength relationship be rethought for these materials, dual phase steel can be processed *via* these methods while realizing the substantial potential in efficiencies.

IV. CONCLUSIONS

The work presented has highlighted some of the implications of transitioning to near net shape casting for dual phase steels compared to conventional thick slab casting. Two casts have been made *via* a laboratory belt cast simulator at 10 mm thickness and rolled to final product of 1 mm thickness and have been compared with a commercial 1-mm-thick product. The following conclusions can be made:

- Using confocal microscopy, the cooling rate dependence of the SDAS was measured for a DP800 steel composition throughout the range of cooling rates applicable to 1/4 thickness position of the cast material from different casting techniques (twin roll, belt, thin and thick slab). It was found that there is very little difference in the SDAS until the cast thicknesses reduces below 50 mm.
- Final product second phase band spacing and, therefore, ferrite grain size is dictated by a balance between the as-cast SDAS and the level of reduction required to produce the final product thickness. The finer SDAS in the thin near net shape casting processes is not enough to account for the lack of reduction to product thickness, and as such the band spacing of final product belt cast material is predicted to be twice as large as final product conventional continuous cast material.
- Tensile testing showed that belt cast material showed poorer properties for both yield strength and UTS, both of which can be accounted for by the difference in grain size. The belt cast samples did, however, show improved elongation and showed equivalent or greater UTS × uniform elongation values.
- Good agreement can be seen between modeling and experimental values for the final properties of the annealed product. The results indicate that steels that are strongly influenced by the second phase band spacing and net rolling reduction for their mechanical properties would inherently give poorer performance when cast *via* near net shape techniques unless compositional modifications are made.

REFERENCES

1. J. Wans, C. Geerkens, H. Cremers, and D. Austermann: in *AISTech—Iron and Steel Technology Conference Proceedings*, vol. 2, 2015, pp. 2626–30.
2. Castrip: http://www.castrip.com/index.html.
3. China's First! Shagang Achieved Industrial Production of Castrip, http://eng.shasteel.cn/doc/2019/05/15/10171.shtml (accessed 15 April 2020).
4. New steel process is faster, lower cost, higher quality, uses 5–10 times less energy and enables new thinner sheets, https://www.nextbigfuture.com/2017/03/new-steel-process-is-faster-lower-cost.html, (accessed 15 April 2020).
5. C. Slater, C. Davis, M. Isac, and R. Guthrie: *Steel Times Int*., 2017, vol. 41, pp. 37–40.
6. S. Ge, M. Isac, and R.I.L. Guthrie: *ISIJ Int*., 2012, vol. 52, pp. 2109–22.
7. S. Ge, M. Isac, and R.I.L. Guthrie: *Progress in Strip Casting Technologies for Steel*; Technical Developments, https://www.jstage.jst.go.jp/article/isijinternational/53/5/53_729/_article (accessed 4 April 2014).
8. M. Daamen, C. Haase, J. Dierdorf, D.A. Molodov, and G. Hirt: *Mater. Sci. Eng. A*, 2015, vol. 627, pp. 72–81.
9. M. Daamen, W. Nessen, P.T. Pinard, S. Richter, A. Schwedt, and G. Hirt: *Procedia Eng*., 2014, vol. 81, pp. 1535–40.
10. L.J. Kecskes, X. Chen, J. Li, V.H. Hammond, Q. Wei, and T.L. Jones: *Evaluation of a Belt-Cast Austenitic Steel Alloy from Salzgitter Mannesmann Forschung: Effect of Hardness on the Ballistic Resistance against Two 0.30-Cal. Projectile Types*, 2017, https://apps.dtic.mil/sti/pdfs/AD1038106.pdf (accessed 15 April 2020).
11. H.-Z. Li, H.-T. Liu, Y. Liu, Z.-Y. Liu, G.-M. Cao, Z.-H. Luo, F.-Q. Zhang, S.-L. Chen, L. Lyu, and G.-D. Wang: *J. Magn. Magn. Mater*., 2014, vol. 370, pp. 6–12.
12. G. Ouyang, X. Chen, Y. Liang, C. Macziewski, and J. Cui: *J. Magn. Magn. Mater*., 2019, vol. 481, pp. 234–50.
13. R. Liang, P. Yang, and W. Mao: *J. Magn. Magn. Mater*., 2017, vol. 441, pp. 511–16.
14. W.-H. Lee, J.-O. Park, J.-S. Lee, J.A. de Castro, and Y. Sasaki: *Ironmak. Steelmak*., 2012, vol. 39, pp. 530–34.
15. K.Y. Xie, L. Yao, C. Zhu, J.M. Cairney, C.R. Killmore, F.J. Barbaro, J.G. Williams, and S.P. Ringer: *Metall. Mater. Trans. A*, 2011, vol. 42, pp. 2199–2206.
16. M. Isac and R.I.L. Guthrie: *Treatise on Process Metallurgy*, Elsevier, New York, 2014, pp. 555–83.
17. Y. Kwon, J.H. Hwang, H.C. Choi, T.T.T. Trang, B. Kim, A. Zargaran, and N.J. Kim: *Met. Mater. Int*., 2020, vol. 26, pp. 75–82.
18. N. Fonstein: *Automotive Steels*, Woodhead Publishing, Cambridge, 2017, pp. 169–216.
19. C. Slater and C. Davis: *LA Metall. Ital*., 2016, vol. February, pp. 23–30.
20. O. Volkova, H.-P. Heller, and D. Janke: *ISIJ Int*., 2003, vol. 43, pp. 1724–32.
21. J. Dobrovska, H. Francova, F. Kavicka, and V. Dobrovska: in *METAL 2010*, Tangier, 2010, pp. 1–6.
22. S.K. Choudhary, S. Ganguly, A. Sengupta, and V. Sharma: *J. Mater. Process. Technol*., 2017, vol. 243, pp. 312–21.
23. D. Zhang: *Characterisation and Modelling of Segregation in Continuously Cast Steel Slab*, Thesis, University of Birmingham, 2015.
24. P.K. Penumakala, A.K. Nallathambi, E. Specht, U. Urlau, D. Hamilton, and C. Dykes: *Appl. Therm. Eng*., 2018, https://doi.org/10.1016/j.applthermaleng.2018.01.121.
25. S. Ge, S. Chang, T. Wang, L.E. Calzado, M. Isac, J. Kozinski, and R.I.L. Guthrie: *Metall. Mater. Trans. B Process Metall. Mater. Process. Sci*., 2016, vol. 47, pp. 1893–1904.
26. Udayraj, S. Chakraborty, S. Ganguly, E.Z.Z. Chacko, S.K.K. Ajmani, and P. Talukdar: *Int. J. Therm. Sci*., 2017, vol. 118, pp. 435–47.
27. T. Zhou: *Control of Microstructure during Solidification & Homogenization of Thin-Slab Cast Direct-Rolling (TSCDR) Microalloyed Steels*, McMaster University, Hamilton, ON, 2010.
28. C. Cicutti and R. Boeri: *Scripta Mater*., 2001, vol. 45, pp. 1455–60.
29. Z.P. Xiong, A.G. Kostryzhev, A.A. Saleh, L. Chen, and E.V. Pereloma: *Mater. Des*., 2015, vol. 88, pp. 537–49.
30. B. Zhu and M. Militzer: *Metall. Mater. Trans. A*, 2015, vol. 46A, pp. 1073–84.
31. C. Slater, M. Ji, B. Bandi, and C. Davis: *Ironmak. Steelmak*., 2020, vol. 47, pp. 496–503.
32. Z.P. Xiong, A.G. Kostryzhev, Y. Zhao, and E.V. Pereloma: *Metals (Basel)*, 2019, vol. 9, p. 449.
33. C. Peng-Heng and A.G. Preban: *Acta Metall*. https://doi.org/10.1016/0001-6160(85)90114-2.
34. Z. Jiang, Z. Guan, and J. Lian: *Mater. Sci. Eng. A*. https://doi.org/10.1016/0921-5093(94)09594-m.
35. S.A. Etesami and M.H. Enayati: *Metall. Mater. Trans. A Phys. Metall. Mater. Sci*., 2016, vol. 47, pp. 3271–76.
36. D. Hull and T.W. Clyne: *An Introduction to Composite Materials*, 2nd ed., Cambridge University Press, Cambridge, 1996.
37. P.D. Basoeki: *MATEC Web Conf*., 2018, vol. 204, pp. 1–8.
38. A. Fillafer, E. Werner, and C. Krempaszky: *Mater. Sci. Eng. A*, 2017, vol. 708, pp. 556–62.
39. B. Mao and Y. Liao: *Mech. Mater*., 2019, vol. 129, pp. 222–29.
40. M. Calcagnotto, Y. Adachi, D. Ponge, and D. Raabe: *Acta Mater*., 2011, vol. 59, pp. 658–70.